Modeling of Active and Passive Nonlinear Metamaterials

P. L. Colestock, M. T. Reiten[1] and J. F. O'Hara[2]

[1]*Los Alamos National Laboratory*

[2]*Oklahoma State University, Electrical & Computer Engineering, Stillwater, OK USA*

(Dated: August 21, 2012)

We develop general results for nonlinear metamaterials based on simple circuit models that reflect the elementary nonlinear behavior of the medium. In particular, we consider both active and passive nonlinearities which can lead to gain, harmonic generation and a variety of nonlinear waves depending on circuit parameters and signal amplitude. We show that the medium can exhibit a phase transition to a synchronized state and derive conditions for the transformation based on a widely-used multiple time scale approach that leads to the well-known Complex Ginzburg-Landau equation. Further, we examine the variety of nonlinear waves that can exist in such systems, and we present numerical results for both active and passive metamaterial cases.

I. INTRODUCTION

The potential of engineered materials that possess novel dielectric and magnetic properties is well known and has been intensively studied in recent years. Much attention has been focused on the properties associated with two- or three-dimensional arrays of subwavelength unit cells comprised of electromagnetic resonators. These so-called metamaterials represent a burgeoning and valuable research area. [1–5] However, comparatively little attention has been given to the case when the resonators themselves possess significant nonlinear properties. Such a situation is akin to that of a lasing medium [6] or nonlinear transmission line [7], which have been found to display a wide variety of frequency and amplitude dependent phenomena.

Moreover, an array of coupled nonlinear oscillators was the basis of the famous Fermi, Pasta, Ulam system [8],[9] that was first studied numerically and found to contain unexpected effects, namely a repeated recurrence of a given initial perturbation, and persistent frequency mixing phenomena. This observation is widely acknowledged to have inspired the modern development of solitons and the very powerful analytical methods for delineating their properties. In addition, very simple nonlinear resonator circuits were shown to exhibit chaos in an isolated context [10], however it is not clear how these complex phenomena might manifest themselves in an array. It is this situation that has compelled us to study nonlinear meta-materials in particular, with an eye to developing novel applications that can make use of these effects. In particular, we are interested in the frequency agility of nonlinear meta-materials, and in identifying the forms of nonlinear waves that may occur in such systems. To this end we have undertaken a theoretical study of nonlinear resonant circuits in the limit where the wavelength is much larger than the cell size. However, the methods we will employ are valid for a broad range of wavelengths.

In general we may divide nonlinear metamaterial arrays into two categories: active and passive. In the active case, the cells contain elements that impart gain to the medium and a source of free energy exists. For our case under study in this work the specific nonlinearity is introduced by the insertion of a biased tunnel diode into the resonator circuit. In the passive category, any nonlinear element which alters its properties with signal amplitude can be considered, and we have chosen to explore the often-used varactor. However, the theoretical methods we apply are general and can be used for virtually any nonlinearity of interest.

In this work, we wish to take advantage of the fact that an array of coupled nonlinear oscillators is essentially the heart of many physical systems of importance in physics and engineering. Plasmas, lasers, superconductors, liquid crystals, even Bose-Einstein condensates among many others, all share characteristics that arise from coupled oscillator arrays. As such, many of the mathematical techniques developed in these fields can find application in the development of viable models for nonlinear metamaterials. In particular, we recognize that all these physical systems generally contain two very disparate time scales: a fast time scale over which the phase of an element may vary, and a slower time scale over which adjacent cells may exchange energy.

By appropriately averaging the fast time scale, we are led to the celebrated Complex Ginzburg-Landau equation (CGLE) [11], developed to explain phase transitions in superconductors. A related set of equations will be developed for our case, and some of its many diverse properties will be found to describe the behavior of these metamaterials. We note that the concept of phase transitions in metamaterials has been introduced by the work of Ref. [12]. They described the behavior of nonlinear permeability and permittivity, which effectively leads to a nonlinear frequency shift and gives rise to interesting hysteresis phenomena. Extensions of this concept to include nearest-neighbor interactions leads to the existence of breather solitons, which have been explored in Refs. [13–23]. This work was focused on passive nonlinearities associated with nonlinear reactances. Our aim in this paper is to extend these concepts in a general way to both active and passive media.

Focusing our attention first on the active case, we begin with the study of a single nonlinear metamaterial cell, developing a circuit model and the dynamical equations describing the behavior of the circuit voltage and current. Our focus is primarily on the behavior of systems which are excited by an external source. Numerical studies indicate the basic operating regimes, and we develop simple analytical results based on the powerful averaging method alluded to above that is widely used for the study of nonlinear systems.

We then apply this technique to an array of nonlinear metamaterial cells, which leads to a system of coupled CGLEs. We explore the nonlinear solutions of these equations, and derive conditions which delineate the various operating regimes based on the choice of system parameters. Full numerical solutions of the equations are presented, which show the diversity of behavior that can be expected in these nonlinear systems. The work is also extended to passive systems, specifically the varactor case, and the results are discussed in the context of potential applications that might be realized.

II. ACTIVE SINGLE-CELL ANALYSIS – TUNNEL DIODE

Many elementary nonlinear resonant circuits have been shown to exhibit complex behavior, such as Chua's circuit [24], among others. We will choose a simple circuit model motivated by metamaterial experiments, and shown in Fig. 1, as it offers the possibility of gain through the negative resistance of a tunnel diode. Such a cell can be realized, for instance, by a split-ring resonator (SRR) loaded with a tunnel diode.[25] Losses are represented by resistor R and the circuit is coupled inductively to its nearest neighbors.

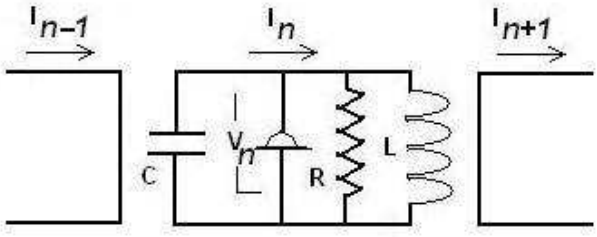

FIG. 1: Circuit model. An RLC circuit includes a parallel tunnel diode.

We note that one may assume both electric as well as inductive coupling, and include effects of signal retardation, which has been studied extensively in linear circuits.[26–28] However, for the purposes of this study, we wish to emphasize the important effects of cell-to-cell coupling, without introducing the complications of additional poles due to the resonances that more general coupling terms will introduce. As such, our

purely inductive coupling model is valid in the limit of long spatial wavelengths relative to the cell spacing. Neglecting the nearest-neighbor interactions altogether for now, we may write the circuit equations as

$$LC\frac{\mathrm{d}^2V}{\mathrm{d}t^2} + V + L\left(\frac{1}{R} + f_1\right)\frac{\mathrm{d}V}{\mathrm{d}t} + 2Lf_2V\frac{\mathrm{d}V}{\mathrm{d}t} + 3Lf_3V^2\frac{\mathrm{d}V}{\mathrm{d}t} = 0 \tag{1}$$

It is well-known that such circuits can exhibit self-oscillations when biased in the negative resistance portion of the tunnel diode current-voltage characteristic. In Eq. 1, we have assumed the usual cubic dependence of the tunnel diode current on voltage, given by

$$I = f_1V + f_2V^2 + f_3V^3$$

and shown in Fig. 2. We can recast the above equation in the form

$$\frac{\mathrm{d}p}{\mathrm{d}t} = -q - \gamma p + \alpha_3 pq^2 \tag{2a}$$

$$\frac{\mathrm{d}q}{\mathrm{d}t} = p \tag{2b}$$

where q is the tunnel diode voltage and p is its rate of change with respect to normalized time, $\tau = \omega_0 t$, and $\omega_0^2 = \frac{1}{LC}$.

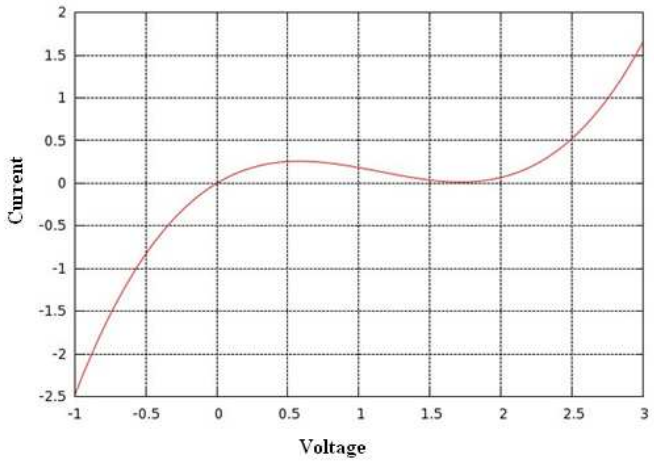

FIG. 2: Tunnel diode I-V characteristic. Negative differential resistance is observed between the voltages of about 0.5 and 1.7 V.

Without loss of generality, we have shifted the voltage reference by $V_0 = -\frac{f_2}{3f_3}$ to remove the quadratic term in the V-I characteristic, tantamount to biasing the tunnel diode. The coefficients to be used in Eq. 2 are then given by

$$\gamma = \left(\frac{1}{R} + f_1 - \frac{f_2^2}{3f_3}\right)\omega_0 L$$

$$\alpha_3 = -3f_3\omega_0 L$$

$f_3 > 0$ which implies α_3 is negative definite and γ may be positive or negative. The key feature of this characteristic is the negative resistance region, while the asymptotes at large amplitudes ensure stability through their associated positive resistance. Fixed points in the dynamics occur when $p = \mathrm{d}p/\mathrm{d}\tau = 0$. There is one such fixed point for this system when $p = q = 0$, however it is also possible that an attractor exists in the form of a limit cycle, depending on parameters. To illustrate this behavior, we transform Eq. 2 into polar coordinates

$$R^2 = p^2 + q^2 \tag{3a}$$
$$q = R\cos\theta \tag{3b}$$
$$p = R\sin\theta \tag{3c}$$
$$\dot{R} = -\gamma\frac{R}{2}(1 - cos2\theta) + \frac{\alpha_3}{4}R^3\sin^2 2\theta \tag{3d}$$
$$\dot{\theta} = -1 - \left(\frac{\gamma}{2} + \frac{\alpha_3 R^2}{2}\sin^2\theta\right)\sin 2\theta + \frac{\alpha_3 R^2}{2}\sin 2\theta \tag{3e}$$

For purposes of illustration, we adopt a straight-forward numerical approach to the integration of the above equations using a standard fourth-order Runge-Kutta method. A typical result for this case is shown in Figure 3. Trajectories are mapped from a random starting point on this plane toward a limit cycle.

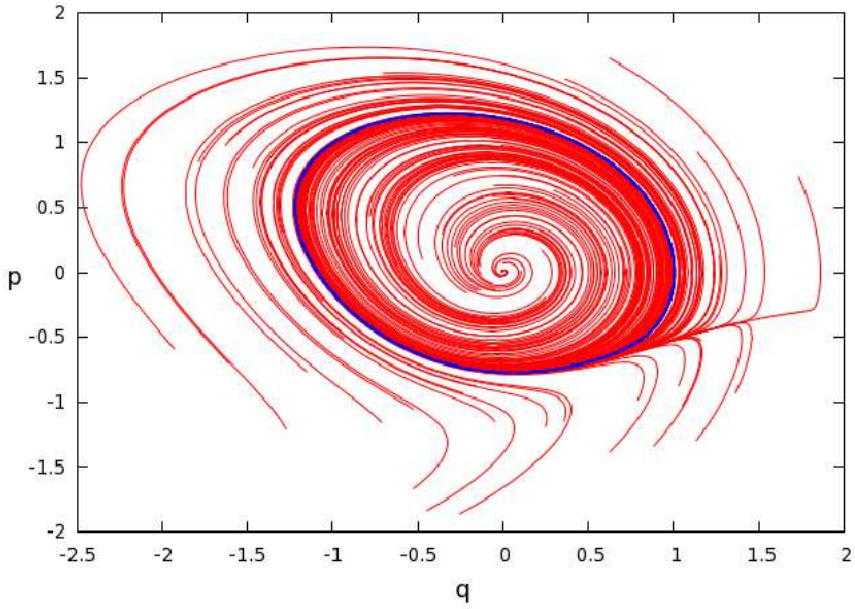

FIG. 3: Phase map of the p-q plane for the self-oscillation case. Trajectories are mapped from random starting points on this plan toward the limit cycle, shown in blue. $\gamma = -1, \alpha_3 = 1$.

It is evident from the $\dot{R}$ equation that a Hopf bifurcation [29] occurs when γ changes sign. Namely, the right hand side of this equation is negative definite when γ is positive (recall that $\alpha_3 < 0$), which gives rise to decaying solutions of the form shown in Fig. 4. However, there is positive growth for some range of small R when γ is negative. That is, there is a bounded region of R values that attracts trajectories from both smaller and larger R regions, hence the existence of a limit cycle.

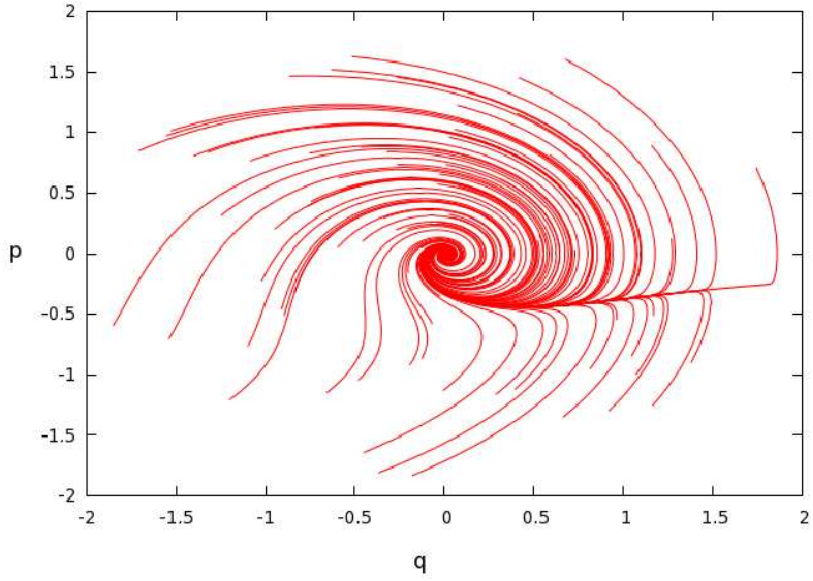

FIG. 4: Phase map of the p-q plane for the damped oscillation case. A Hopf bifurcation occurs as γ changes sign, creating the limit cycle of Fig. 3. $\gamma = 1, \alpha_3 = 1$.

In this work we shall be primarily interested in the case when the SRR cells are illuminated by an external source, which can be added, with appropriate scaling, as a time-dependent term on the right hand side of Eq. 1. In that case we may expect the response to be characterized by the self-oscillation frequency, the external drive frequency and possibly sums and differences of these. This is indeed the case as shown in Fig. 5.

Significantly, we observe an amplitude dependence of the response such that sufficiently large drive amplitudes tend to lock the response to the drive frequency, suppressing significant harmonic generation, as shown in Fig. 6. This is a key finding of our analysis, namely at sufficiently large signal amplitude, an external source can abruptly synchronize all the elementary resonators to the drive frequency and the relative phase of all oscillators becomes bounded. [30] We will find analytic conditions for this transition in Section III.

It is of interest to determine whether the circuit driven by an external source can exhibit chaotic behavior. A phase plane diagram of the dynamics in the transition region of Fig. 6 suggests that this may indeed be the case, as shown in Fig. 7. However, the frequency spectrum of Figs. 3 and 4 contains only narrow lines, which suggests that the system is quasiperiodic, rather than truly chaotic, namely that it contains a finite number of incommensurate frequencies.

It is worthwile to explain further what is meant by these terms. Following Ref. [29], we expect that driven systems will contain the drive frequency and possibly a self-oscillation frequency, if it can exist, along with harmonics and sums and differences of these frequencies, when there are nonlinearities. This behavior is called quasiperiodic, because if the frequencies happen to be rational multiples of each other, the system will be exactly periodic on some time scale. For irrationally related frequencies, there is strictly no such periodicity, but the system may be arbitrarily close to such a condition and the system maintains a certain regularity. For truly chaotic systems, no such periodicity occurs and typically the spectral response is a broad spectrum lacking any significant line structure. Clearly the distinction between chaos and quasiperiodicity is imprecise, and a given system must be categorized according to the application at hand.

To elucidate this behavior further, it is useful to use a Poincaré Surface-of-Section, as shown in Fig. 8. The voltage is sampled once per cycle of the drive voltage and displayed over many cycles of the response.

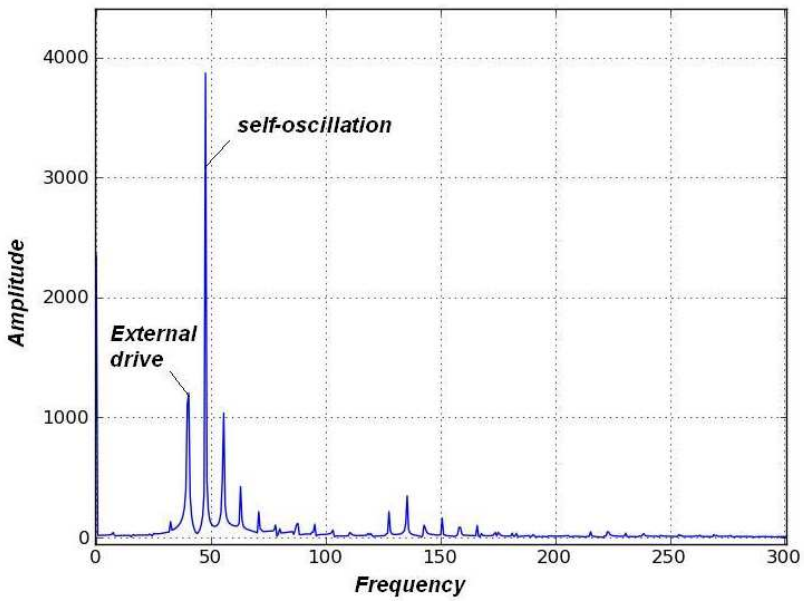

FIG. 5: Spectral response for excitation slightly below the self-oscillation frequency. The only frequencies which appear in the system are those of the drive, the self-oscillation frequency, and their sums and differences.

When the circuit is locked to the drive at large drive amplitudes, the resulting display is confined to a single, narrow line representing synchronous phase. At lower drive amplitudes, there are bands of either quasiperiodic or chaotic behavior. Some regions of detailed structure in this plot suggest a finite number of frequencies exist, which we denote as quasiperiodic regions. The associated frequency spectrum is comprised of a collection of narrow, but nonrational, lines. The system is also characterized by an unbounded phase difference between the drive and self-oscillation frequencies, resulting in a spread of sampled signal levels. True chaotic behavior does not necessarily occur, which is difficult to determine with such a plot. We will return to this subject in the next section when we consider arrays of nonlinear cells and develop conditions for the transitions that can be observed in these numerical results.

It is worthwhile to note that further analytical results based on the study of Eq. 2 or Eq. 3 are not generally achievable. However, because of the tendency for the system to approach periodic behavior on the limit cycle, or for it to decay slowly toward the fixed point in the damped case, it is feasible to split the time behavior into a fast oscillatory part coupled with the slow evolution of the amplitude. This two-time scale feature is the basis for a powerful analytical approach [29, 31, 32] that permits much more of the system behavior to be delineated.

III. ARRAYS OF NONLINEAR SRR CELLS

An application of particular importance is an array of nonlinear split-ring resonators of the type considered in Sec. II. As mentioned in the introduction, we will find the properties of such arrays fall into two categories: that of active, gain-containing structures and those structures that while nonlinear, are predominantly passive and must be driven externally to generate a nonlinear response. As was the case in the previous single-cell analysis, we restrict our attention to that of externally-driven arrays, active or passive, and we ask the question as to what dynamical regimes may occur, and which circuit parameters are responsible for

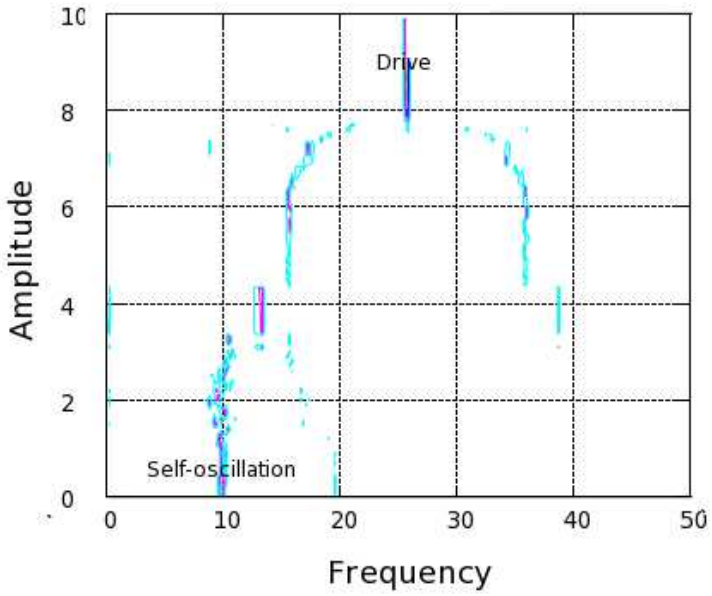

FIG. 6: Contour plot of synchronization as a function of drive amplitude. The colors represent levels associated with the narrow line structure in the frequency spectrum. As the drive amplitude is increased from low level, the self-oscillation lines coalesce and disappear at Hopf bifurcation points. Above a critical drive amplitude, the self-oscillations are completely suppressed, and the response becomes entrained to the drive signal.

delineating the boundaries of these regimes.

In the following, we will first describe the multiple time scale approach we are taking to construct a model of a nonlinear array of SRRs, and we will apply this approach to both active and passive SRR arrays in turn. This will lead to a simplified set of dynamical equations from which many properties of the arrays can be deduced.

A. Weak nonlinear analysis: the method of averaging – asymptotic results

The fast time scale of a nonlinear cell is associated with the phase variation of the resonator operating near its resonant frequency, while the slow time scale is associated with the variation of the envelope of these oscillations. In particular, we are most interested in the transition point where self-oscillations are just initiated as we change a parameter in the circuit, for instance the growth rate, γ, in Eq. 2. Formally this circumstance corresponds to an expansion of the time derivative of the form

$$\frac{\partial}{\partial t} = \frac{\partial}{\partial \tau_0} + \varepsilon \frac{\partial}{\partial \tau_1} + \cdots$$

where $\tau_0 \ll \tau_1$ and ε is a small parameter. A formal expansion procedure leads to an asymptotic representation of the solution, namely one which is valid for times of order τ_1 or longer. As we show in Appendix A, for cases near the onset of self-oscillations, an appropriate expansion parameter is the growth rate γ. However,

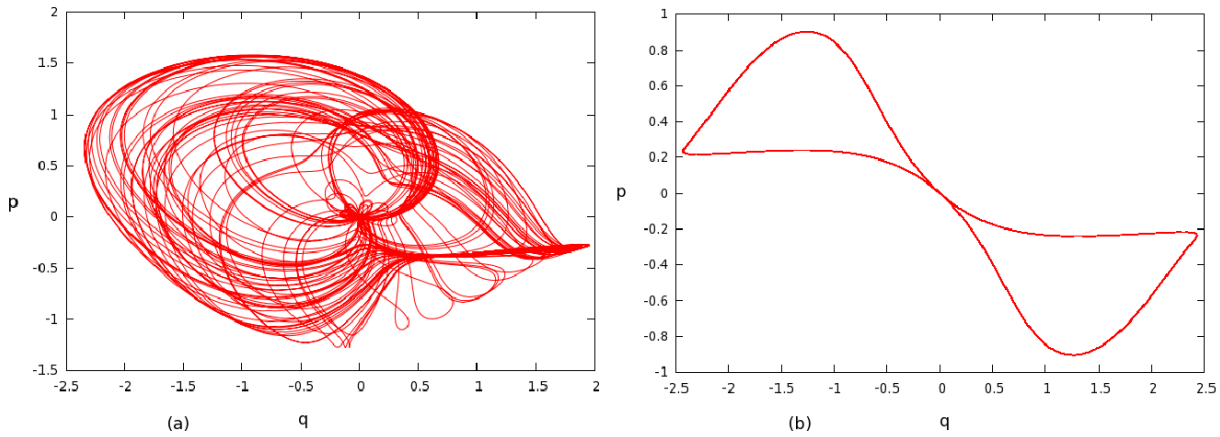

FIG. 7: Phase plane representation of driven system. (a) quasiperiodic behavior below synchronization threshold (b) synchronized oscillations above threshold.

for quasiperiodic oscillatory systems, we may equivalently take each quantity to be comprised of a fast phase variation combined with a slowly-varying envelope function of the form

$$A(t) = A(\tau_1)\, \mathrm{e}^{i\omega\tau_0} + \mathrm{c.c} \tag{4}$$

where ω is the arbitrary carrier frequency, to be conveniently chosen to facilitate the particular analysis at hand. The ansatz Eq. 4 can be thought of as the first term of a Fourier series representation. We shall consider a more general form in Sec. IV. After substitution, we then multiply by $\mathrm{e}^{-i\omega\tau_0}$ and average over one cycle of the fast time scale, keeping the slowly-varying term constant. This procedure selects the ω frequency component, including all those frequencies which mix to this frequency through nonlinear interactions. We may apply such a procedure to the single SRR cell described in Section II, keeping only the fundamental frequency terms for now, which results in the equation for the envelope A (see Appendix A)

$$i\omega\frac{\partial A}{\partial \tau_1} - \left(\omega^2 - 1\right) A + i\omega\gamma A - i\omega\frac{\alpha_3}{4} A|A|^2 = 0 \tag{5}$$

We note that the third term represents growth or decay and may exhibit gain if γ is negative. The fourth term quenches the growth and causes saturation at sufficiently large amplitudes. Supressing the subscript on τ, we may rewrite Eq. 5 as

$$\frac{\partial A}{\partial \tau} + \left(\gamma - i\frac{1-\omega^2}{\omega}\right) A - \frac{\alpha_3}{4} A|A|^2 = 0 \tag{6}$$

This equation may be readily solved if we let $A = R\,\mathrm{e}^{i\theta}$, yielding the two equations

$$\dot{R} = -\gamma R + \frac{\alpha_3}{4} R^3 \tag{7a}$$

$$\dot{\theta} = \frac{1-\omega^2}{\omega} \tag{7b}$$

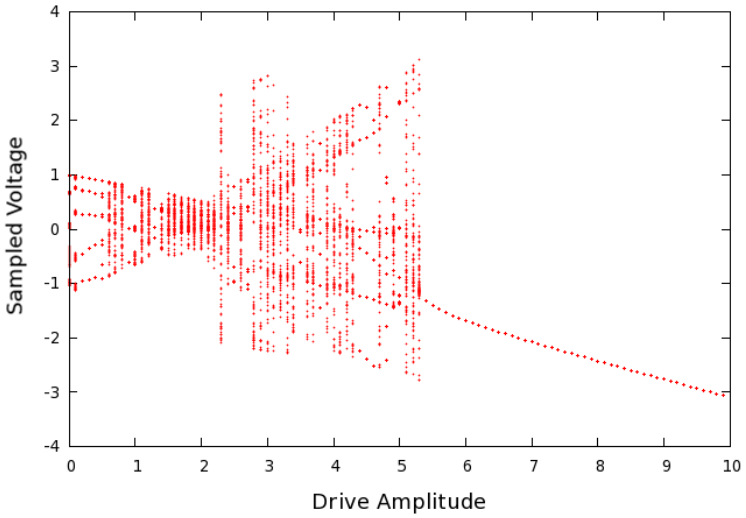

FIG. 8: Poincaré surface-of-section for a driven system depicting bands of quasiperiodic behavior at low drive amplitudes, when two or more incommensurate frequencies coexist in the circuit response. The drive frequencyis 0.5 relative to unity for the self-oscillation frequency. At a drive amplitude of approximately 5.4 units, the system becomes phase-locked to the external driving force. This transition amplitude is a function of the detuning parameter value.

which have the exact solutions

$$R^2 = \frac{R_0^2\, \mathrm{e}^{-2\gamma\tau}}{1 - \dfrac{\alpha_3 R_0^2}{4\gamma}(1 - \mathrm{e}^{-2\gamma\tau})} \tag{8a}$$

$$\theta = \left(\frac{1-\omega^2}{\omega}\right)\tau + \theta_0 \tag{8b}$$

We note the similarity between Eq. 3 and Eq. 7. Both describe the limit cycle behavior of the dynamical equations, but the averaging technique singles out the fundamental harmonic, effectively decoupling the phase and amplitude equations. In particular, note that the second of these implies that the motion is isochronous, namely that the phase of the oscillator is independent of the amplitude. This is a special result for the case of Eq. 6, where we have dropped coupling to higher harmonic terms. It is also a consequence of the fact that the tunnel diode characteristic we have assumed introduces gain through a nonlinear resistance, but does not include a nonlinear frequency shift. It is in fact this condition of isochronicity which ensures that the motion is quasiperiodic, rather than truly chaotic. In order to find chaotic behavior, we must either assume a nonlinear reactance or include higher harmonic terms in the multiple time scale expansion, and we will return to this topic in Section IV.

Note that the steady-state occurs at an amplitude

$$R^2 = \frac{4\gamma}{\alpha_3} \tag{9}$$

which shows that a limit cycle is achieved for $\gamma < 0$ associated with a monotonically increasing phase, consistent with the numerical results in Sec. II.

As noted above, of particular practical interest is the driven solution; specifically we assume a sinusoidal forcing term on the right hand side of Eq. 6. In particular, we assume the drive frequency is near the carrier frequency ω where it influences both the amplitude and phase of the envelope function A. Namely it is taken to be of the form $\varepsilon\, \mathrm{e}^{i\Omega\tau}$, where $\Omega << \omega$ and represents a small deviation from the carrier frequency and ε is an amplitude parameter. Upon separating into real and imaginary parts, we arrive at

$$\dot{R} = -\gamma R + \frac{\alpha_3}{4} R^3 + \varepsilon \cos(\Omega\tau - \theta) \tag{10a}$$

$$\dot{\theta} = \frac{1-\omega^2}{\omega} + \varepsilon \sin(\Omega\tau - \theta) \tag{10b}$$

If we further define $\psi = \Omega\tau - \theta$, the phase equation becomes

$$\dot{\psi} = \Omega - \frac{1-\omega^2}{\omega} - \varepsilon \sin(\psi) \tag{11}$$

which defines the evolution of the phase difference between the forcing term and the oscillator. Defining ν as the detuning parameter

$$\nu = \Omega - \frac{1-\omega^2}{\omega}$$

we can recognize this equation as being related to that of the nonlinear pendulum, and note that it exhibits a critical transition point when $|\varepsilon/\nu| = 1$. If we sample the resulting phase variation at the same point in each forcing function cycle, we obtain the well known *circle map* [29]

$$\psi_{n+1} = \psi_n + \nu - \varepsilon \sin(\psi_n) \tag{12}$$

The primary consequence of this result is that the phase can exhibit an abrupt transition from monotonic behavior to *entrainment or synchronization* within the driving function phase. In other words, at low values of ε, the oscillator responds at its self-oscillation frequency, which is in general, incommensurate with the driving frequency. The phase difference increases without bound, and both frequencies are present in the system response. As ε is increased, or as the detuning parameter is varied closer to a resonance condition, synchronization abruptly occurs and the phase difference is bounded by 2π. The global map of synchronization for the circle map is shown in Fig. 9. Synchronization occurs in the shaded region associated with the rational harmonic known as the Arnold tongue. The phase difference between the drive and the circuit response remains bounded in time. The reader is referred to the rich literature on this subject for further detail.[29] We note that this behavior represents well the results found by direct integration of the circuit equations discussed in Sec. II.

B. Nearest neighbor interactions

Up to now, we have neglected the interaction of nearby SRR cells, which may occur from both electric and magnetic fields. For simplicity, we consider only magnetic coupling in this paper, but the analysis is easily extended to include electric field coupling as well.

Referring to the circuit equations, Eq. 1 , the addition of mutual coupling terms gives rise to additional terms of the form

$$V_n = L\frac{\mathrm{d}I_n}{\mathrm{d}t} - M\frac{\mathrm{d}I_{n-1}}{\mathrm{d}t} - M\frac{\mathrm{d}I_{n+1}}{\mathrm{d}t} \tag{13}$$

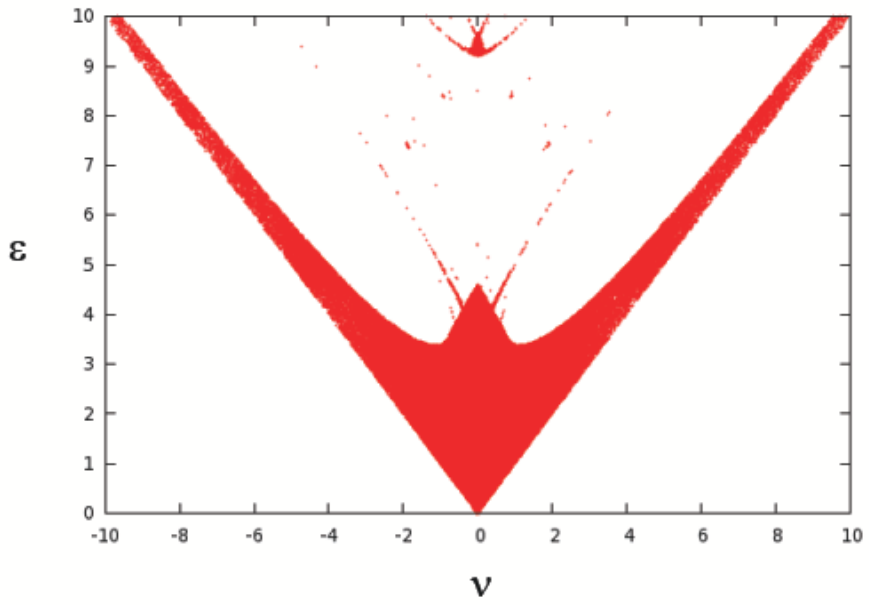

FIG. 9: Circle map showing a region of synchronization where the phase difference of self-oscillation and external drive is bounded. The parameter ϵ represents the drive amplitude and ν corresponds to frequency detuning between the drive and the self-oscillation frequencies.

where we have assumed that the mutual inductance is symmetric, though such an assumption is not strictly necessary. Adding and subtracting $2M/L$ in Eq. 1 and passing to the continuum limit, we arrive at the following equation for the envelope

$$\left[i\frac{\partial}{\partial\tau} + i\gamma + \frac{1-\omega^2}{\omega} - \frac{\partial^2}{\partial z^2}\right] A - i\frac{\alpha_3}{4}A|A|^2 = 0 \tag{14}$$

which is a form of the celebrated Complex Ginzburg-Landau equation (CGLE) [11]. To arrive at this form, we have scaled the variables in the following way

$$z = x\sqrt{\frac{L}{M} - 2}$$
$$\omega_0 \to \omega_0\sqrt{1 - 2\frac{M}{L}}$$

Moreover, we may rescale time to remove the term proportional to A. It has been shown [29] that that the dynamical equations for virtually any nonlinearity with weak coupling will lead to an equation of the form of Eq. 14. In the following, we will describe a procedure to identify all the possible nonlinear waves that might exist in the system. At this point we are still neglecting all coupling to higher-order harmonics, but they will be included in Sec. IV.

C. Traveling wave solutions

The CGLE given by Eq. 14 has received an enormous amount of attention in the literature, as it pertains to many interesting physical systems. It is known to exhibit solitons, shocks, and domain wall solutions, among others. We note that this behavior was anticipated by the work of Shadrivov [33] and others [13–15], whose results we will extend in the following. The form we have derived is not the most general, as we have noted in the previous section, because, due to our neglect of harmonic coupling, it lacks a nonlinear frequency shift term. Nonetheless, the methods we shall employ to investigate its behavior are general and may be used for other situations of interest.

We begin with the assertion that the most important solutions of the CGLE in this context are traveling waves of the form

$$A = \mathrm{e}^{i\phi(z-\nu_0\tau)-i\hat{\Omega}\tau}a(z-\nu_0\tau) \tag{15}$$

where $\hat{\Omega}$ and v_0 are parameters we have introduced to permit matching appropriate boundary conditions at infinity. Following the procedure described in reference [34], we substitute this into Eq. 14 which leads to the following set of ordinary differential equations

$$\psi' = \gamma - (\nu_0 + 2\psi)k - \frac{\alpha_3}{4}a^2 \tag{16a}$$

$$k' = \psi^2 + \nu_0\psi + \hat{\Omega} - k^2 \tag{16b}$$

$$a' = ka \tag{16c}$$

with the further definition $\psi = \phi'$ and the prime refers to differentiation with respect to the traveling wave argument. Note that the $\frac{1-\omega^2}{\omega}$ term has been incorporated into the definition of $\hat{\Omega}$. We wish to analyze the properties of Eq. 16 as a dynamical system and are specifically interested in solutions which connect fixed points in the three-dimensional parameter space. These points are namely those in which the functions a or k are constant as $z - \nu_0\tau \to \pm\infty$. Following Saarloos and Hohenberg [34], we note that there are two kinds of fixed points of interest:

$$\begin{aligned} \text{Linear}: &\quad a = 0,\ k \neq 0 \\ \text{Nonlinear}: &\quad a \neq 0,\ k = 0 \end{aligned}$$

Valid solutions are found by integrating Eq. 16 from one fixed point to another where the parameters $\hat{\Omega}$ and ν_0 serve to satisfy appropriate trajectory boundary conditions. We find shock, or front, type solutions that join an L point to an N point, solitons which join a pair of L points to each other, and domain wall solutions which join a pair of N points. For the above case, we may plot the fixed point map as shown in Fig. 10. Each fixed point in turn must be analyzed for stability properties by linearizing Eq. 16 about the fixed point. We find three eigenvalues in each case which determine directions of stability or instability passing into or out of the fixed points. By simple counting arguments, we can find a finite set of solutions that represent all the traveling waves supported by the system. We note that shocks, solitons and domain wall solutions are all possible for our system. For the L fixed point case, the stability equation is given by

$$(\lambda - k_L)\left(\lambda^2 + 4\lambda k_L + 4k_L^2 - \frac{2\psi_L\gamma}{k_L} + \frac{\gamma^2}{k_L^2}\right) = 0 \tag{17}$$

where k_L is the solution of $k_L^2 = \psi_L^2 + \psi_L\nu_0 + \hat{\Omega}$ with $\psi_L = \gamma/2k_L - \nu_0/2$. As such, we see that one or two eigenvalues are stable, while the rest are unstable. Similarly, for the N fixed points, one, two or three eigenvalues are stable. A viable solution of the CGLE is then formed by finding the trajectory in the three-dimensional parameter space of Eq. 16 that connects an unstable eigendirection of one fixed point to

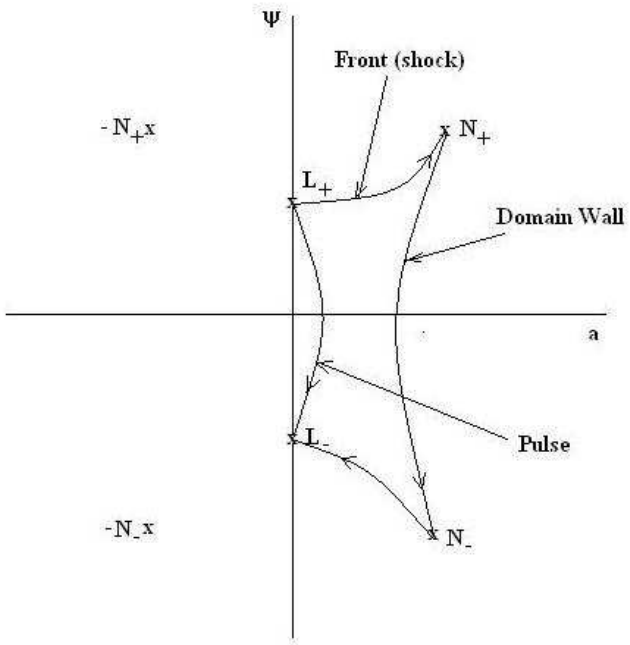

FIG. 10: Fixed point map for the traveling wave solution space.

the stable eigendirection of another. Varying the parameters Ω and ν_0 ensure that both endpoint conditions can simultaneously be met.

For definiteness, we consider the case of a trajectory beginning at an L fixed point and ending at an N fixed point, as it represents the transition from an initially unexcited state to one which satisfies the steady-state condition given in Eq. 9. We note here that this procedure does not indicate how the system evolves into a given nonlinear mode from any given initial condition, nor whether an allowable solution may be excited by any means. But it does identify all consistent travelling wave solutions. Using the following boundary conditions

$$\begin{aligned}
&\text{L point :}\\
&\qquad a_L = 0\\
&\qquad k_L = \pm\sqrt{\frac{\hat{\Omega} - \frac{\nu_0^2}{4} + \sqrt{\left(\hat{\Omega} - \frac{\nu_0^2}{4}\right)^2 + \gamma^2}}{2}}\\
&\text{N point :}\\
&\qquad a_N^2 = -\frac{\gamma}{c_0}\\
&\qquad \psi_N = \frac{-\nu_0 \pm \sqrt{\nu_0^2 - 4\hat{\Omega}}}{2}
\end{aligned}$$

we integrate Eqs. 16 numerically, producing a shock front as shown in Fig. 11.

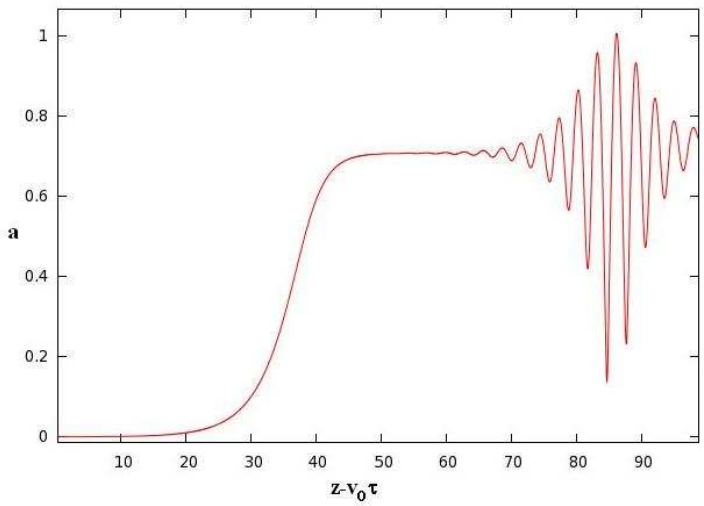

FIG. 11: Solution of an L→N transition showing a basic shock front solution. However a soliton is also produced on the plateau region as the trajectory encircles the stable fixed point. Its generation is indicative of an instability associated with the steady-state plane wave solution.

We note however that a pulse-like, or soliton solution occurs on the plateau as the trajectory encircles the stable N-type fixed point. This suggests that the plane wave solution associated with the steady state is potentially unstable. That this is indeed the case can be established by linearizing the spatio-temporal case given in Eq. 14. That is, letting $R = 1 + \rho$ and dropping all higher order terms leads to

$$-\dot{\theta} + \rho - \rho'' = 0 \tag{18a}$$

$$\dot{\rho} + \gamma\rho - \theta'' = 0 \tag{18b}$$

Applying the Fourier transform to these linear equations leads to the dispersion relation in the Fourier-transformed variables $\tilde{\omega}$ and $\tilde{k}$

$$\begin{vmatrix} \gamma - i\tilde{\omega} & \tilde{k}^2 \\ 1 + \tilde{k}^2 & i\tilde{\omega} \end{vmatrix} = 0$$

with the solution

$$\tilde{\omega} = \frac{-i\gamma \pm i\sqrt{\gamma^2 - 4\tilde{k}^2(1 + \tilde{k}^2)}}{2}$$

which implies instability whenever $\gamma < 0$. Note that this condition is precisely the condition for the appearance of a Hopf bifurcation found in Sec. II. This result can be recognized as the Benjamin-Feir instability [35] associated with long wavelength water waves. These results will be confirmed by direct numerical computation of Eq. 14 in the next section.

D. Numerical results

As was done in previous sections, we shall focus in this section on the question of how such metamaterials respond to excitation by an external source. We have seen how single cells can become phase-synchronized

by an external forcing term. We note that identical behavior is expected from an array of oscillators when the cells are uncoupled from one another. We now wish to consider an array that is excited by a localized external source in the form of a Gaussian beam, including inter-cell coupling. We shall first consider the one dimensional case composed of a string of nonlinear cells and employ a partial differential equation solver with comprehensive error-checking [36] to Eq. 14. The excitation beam is initiated at $t = 0$ and constrained to the center of the linear array. Only the fundamental behavior is considered first.
Boundary conditions are taken to give $\partial A/\partial z = 0$, though this choice is not critical. Integration is carried out using a high-order finite element method.[36] Error tolerance is set to 10^{-5} and up to 5×10^5 unknowns are used. The time evolution of the solution is shown in Fig2. 12 for the case $\gamma < 0$, and $4\gamma/\alpha_3 = 0.5$.

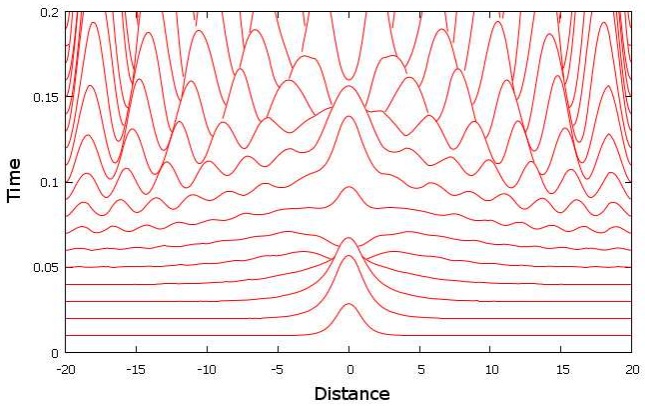

FIG. 12: Early time evolution of the array response for the $\gamma < 0$ case to a Gaussian beam source on a linear array of nonlinear oscillators depicted as a waterfall plot. Time proceeds upward in equal increments, with the envelope A^2 plotted vertically for each time step. The Gaussian beam is seen to split into two outward propagating fronts that generate solitons as they encounter the boundaries, which then propagate back into the center.

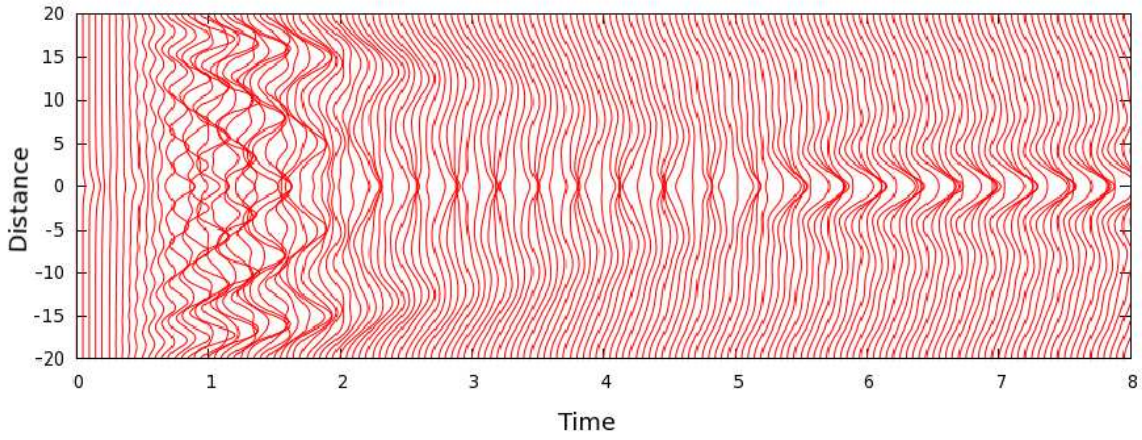

FIG. 13: Long time behavior of the array response for the $\gamma < 0$ case depicted in Fig. 12. Time proceeds left to right in equal increments, with the envelope A^2 plotted horizontally for each time step. The long time response consists of the synchronized steady state augmented by continuous low amplitude soliton generation by the Gaussian beam.

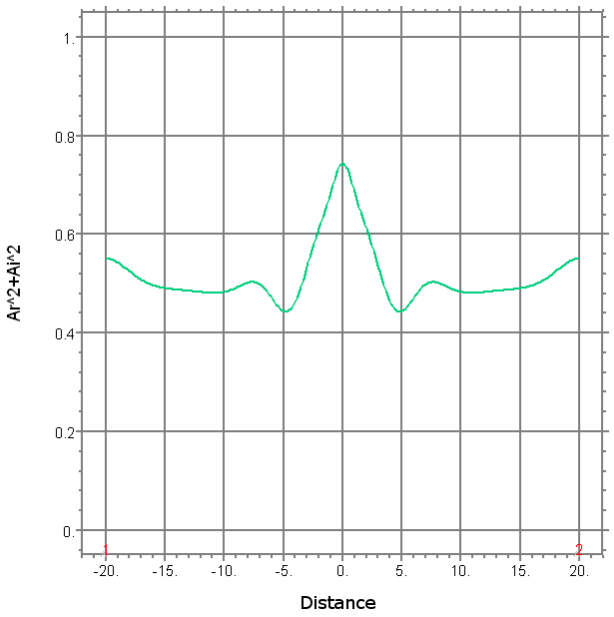

FIG. 14: Profile of the envelope A^2 at late times showing the steady state condition achieved superimposed with the Gaussian drive amplitude. The asymptotic value described in the text for this case is $A^2 = 0.5$. Slight deviations from the steady-state value are observed at the boundaries where the derivative is imposed to be zero.

We see that the initial Gaussian splits into left- and right-going fronts with a plateau at the steady state value ($A^2 = 0.5$). Upon encountering the boundaries, the fronts show the generation of a short-wavelength solitary wave which reflects back into the array. The amplitude and wavenumber of this oscillation gradually decrease until a synchronized, quasi steady-state is reached. The late-time solution achieves a steady state superimposed with the drive beam, as shown in Fig. 14. The Gaussian excitation then continues to excite low amplitude waves and the function assumes a steady perturbation at the boundaries. By comparison, we note that for the $\gamma > 0$ case, only a steady response associated with the Gaussian illumination profile is produced. This is consistent with our asymptotic analysis in Section III A. In Fig. 15 we show results for the two-dimensional case which is formed by extending the spatial operator to two spatial dimensions. The circuit parameters are otherwise unchanged. The results are essentially similar to the one-dimensional case. No spiral features or other exotic waves are observed, consistent with our finding that the dynamic of these waves is predominantly isochronous.

However we observe that the plateau, particularly the front component, is unstable when the growth rate, γ is increased, as shown. In general, we find that the boundaries have the tendency to generate short-wavelength modes, albeit transiently, in the approach to the steady state.
Another interesting result is obtained when the boundaries are asymmetric, namely when the function A is constrained to zero at one edge. The results, shown in Fig. 16, indicate a single soliton is generated at the $A = 0$ boundary, which then propagates through the domain until it encounters the (upper) boundary where $\partial A/\partial z = 0$. It then becomes pinned at that boundary and a steady state is reached.

IV. HARMONIC BEHAVIOR

We now return to the question of how such arrays behave in the presence of multiple harmonics. Essentially, we wish to reproduce the behavior we have seen in the single cell numerical solutions, but include the effects

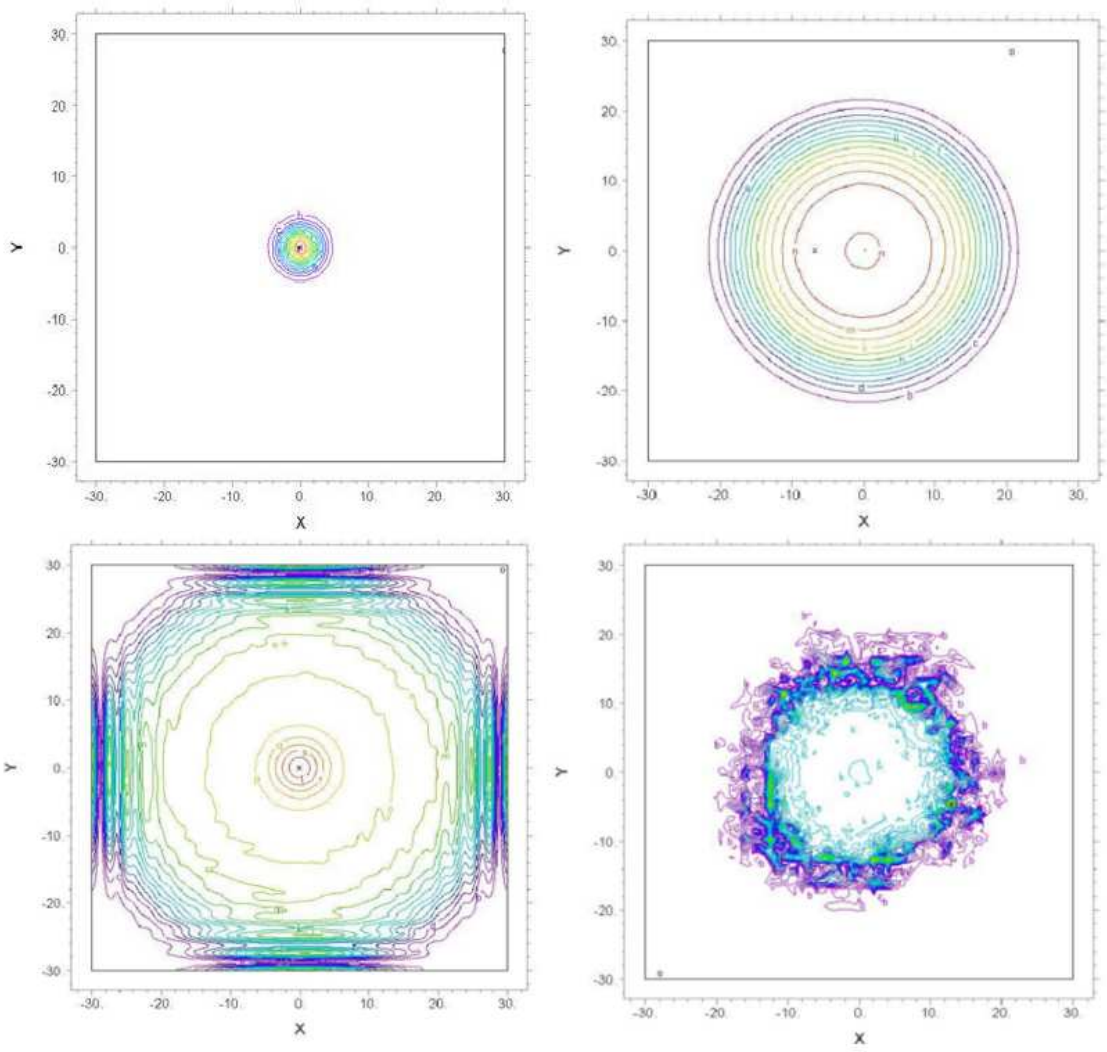

FIG. 15: Two-dimensional numerical results for the tunnel diode case with $\gamma < 0$ using a finite element method with error tolerance set to 10^{-5}[36]. Snapshots are shown at the start of the calculation, upper left, after the formation of the plateau, upper right, during the interaction of the front with the boundaries, lower left, and for a larger growth rate, lower right.

of nearest neighbor coupling. Specifically we will employ the averaging method described in the previous section to a series of harmonics and modes.

We begin with the ansatz that permits multiple harmonics to exist for each nonlinear mode

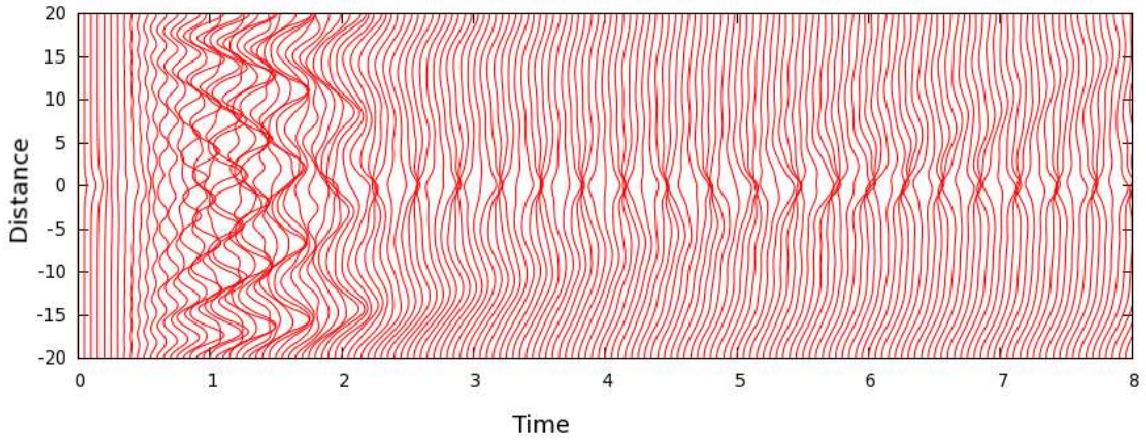

FIG. 16: Waterfall plot of the behavior of the envelope A with asymmetric boundary conditions. The plateau encounters the boundary by generating short wavelength modes followed by a single soliton generated at the $A = 0$ boundary which propagates to the left, finally becoming pinned at the $\partial A/\partial z = 0$ boundary.

$$V_j = \sum_{k=1}^{N} A_{jk}\, \mathrm{e}^{ik\omega t} + \sum_{k=1}^{N} A_{jk}^{*}\, \mathrm{e}^{-ik\omega t} \tag{19}$$

where V_j is the voltage associated with the j^{th} mode of the nonlinear cell. In this work, we have assumed that only one such spatial mode exits in a given cell, but in general multiple modes may occur. The method of averaging applies to the general case, but in this work we will continue to consider only one spatial mode which, however, can support a series of harmonics typical of a nonlinear circuit. We will drop the j subscript in the subsequent analysis. Upon substitution into the circuit equation, Eq. 1, along with the nearest neighbor coupling terms, Eq. 13, we carry out the average over a cycle to obtain a coupled system of Complex Ginzburg-Landau equations, one for each harmonic.

$$\begin{aligned} i\omega n\dot{A}_n - \left[n^2\omega^2 - \omega_0^2\left(1 - 2\frac{M}{L}\right)\right] A_n + \frac{i\omega n}{C}\left(\frac{1}{R} + f_1\right) A_n - \frac{M}{L}\frac{\partial^2}{\partial z^2} A_n = -in\omega\frac{f_2}{2C}\left\langle \phi^2 - \phi^{*2}\right\rangle_n \\ - in\omega\frac{f_3}{4C}\left\langle \phi^3 - \phi^{*3} + \phi^*\phi^2 - \phi\phi^{*2}\right\rangle_n, \qquad n = 1\ldots N \end{aligned} \tag{20}$$

where $\phi = \sum_{k=1}^{N} A_k\, \mathrm{e}^{ik\omega t}$ and the brackets $<>_n$ imply that the n^{th} harmonic is kept in the averaging. The coefficients for up to $n = 5$ harmonics are documented in Appendix B. In reality, two or three harmonics are usually adequate to represent the important mechanism of *three-wave mixing* or *parametric coupling*. Eq. 20 is the primary result of this study and it represents the spatio-temporal evolution of the frequency spectrum for our active, tunnel-diode based nonlinear system. In the limit of mono-frequency, it exhibits the CGLE behavior discussed in previous sections. In the limit of a spatially uniform solution, such as that associated with the plateau discussed previously, it yields a system of parametrically-coupled oscillators. Writing out the equations for the two harmonic case where we have once again taken $f_2 = 0$ and scaled both space and time to simplify the equations, we find

$$\left\{1-\alpha^2-\frac{\partial^2}{\partial z^2}+i\frac{\partial}{\partial\tau}+i\gamma\right\}A_1=-ic_0\left(A_1|A_1|^2+2A_1|A_2|^2\right)+E_1 \tag{21a}$$

$$\left\{1-4\alpha^2-\frac{\partial^2}{\partial z^2}+2i\frac{\partial}{\partial\tau}+2i\gamma\right\}A_2=-2ic_0\left(2A_2|A_1|^2+2A_2|A_2|^2\right) \tag{21b}$$

where

$$\gamma=\frac{\omega}{\omega_0^2\left(1-2\frac{M}{L}\right)C}\left(1/R+f_1\right) \tag{22a}$$

$$c_0=\frac{3f_3\omega}{4C\omega_0^2\left(1-2\frac{M}{L}\right)} \tag{22b}$$

$$\alpha^2=\frac{\omega^2}{\omega_0^2\left(1-2\frac{M}{L}\right)} \tag{22c}$$

where E_1 represents the $n=1$ harmonic of the driving source. The structure is manifestly the same as that of the single harmonic CGLEs, except that the coupling terms break the symmetry of the power flow and add a nonlinear frequency shift. This is precisely what is needed to produce a band of true chaotic behavior. Such a system can produce chaotic behavior at sufficiently high driving amplitudes. Moreover, driving the system at precisely the difference harmonic between A_1 and A_2 as shown in the above example could be expected to produce resonant behavior and enhanced harmonic generation.

We find it is most convenient to solve Eq. 21 numerically, and the results are shown for the one-dimensional case in Fig. 17 and Fig. 18. We find the coupling to the harmonics to be sufficiently weak so that the fundamental CGLE behaves in a manner similar to the single-frequency case. However the third harmonic shows complex spatial dependence associated with distributed coupling from the drive plus fundamental harmonic. No second harmonic excitation occurs in this case because of the odd symmetry of the nonlinear coupling terms. In particular we note that the system tends toward a steady state where the derivative terms in Eq. 21 are set to zero. The results indicate that the steady state is a detailed balance between the growth rates at each harmonic and the coupling terms which tend to distribute power across frequency.

V. PASSIVE CASE – VARACTOR

In the case of a passive metamaterial, no gain is present in the medium. However nonlinearity can still produce interesting phenomena by frequency mixing. A typical varactor-based metamaterial cell is shown in Fig. 19.
The most important feature of such a circuit is the fact that the reactance is nonlinear with amplitude, thereby introducing a nonlinear frequency shift. The circuit equation can be written as

$$LC(V)\frac{\mathrm{d}^2V}{\mathrm{d}t^2}+\frac{L}{R}\frac{\mathrm{d}V}{\mathrm{d}t}+L\frac{\partial C}{\partial V}\left(\frac{\mathrm{d}V}{\mathrm{d}t}\right)^2+\left(1-2\frac{M}{L}\right)V-\frac{M}{L}\frac{\partial^2V}{\partial x^2}=0 \tag{23}$$

Again neglecting the spatial and all harmonic coupling for the moment and going through a similar analysis as that carried out for the active case, we find the following averaged equation for the envelope of a single cell

$$i\frac{\partial A}{\partial\tau_1}-\frac{(\omega^2-\omega_0^2)}{\omega}A+i\gamma A\left(1+\frac{\beta^2C_1^2}{C_0^2}|A|^2\right)+\frac{\beta^2C_1^2}{C_0^2}\left(\frac{\omega_0^2+\omega^2}{\omega^2}\right)A|A|^2=0 \tag{24}$$

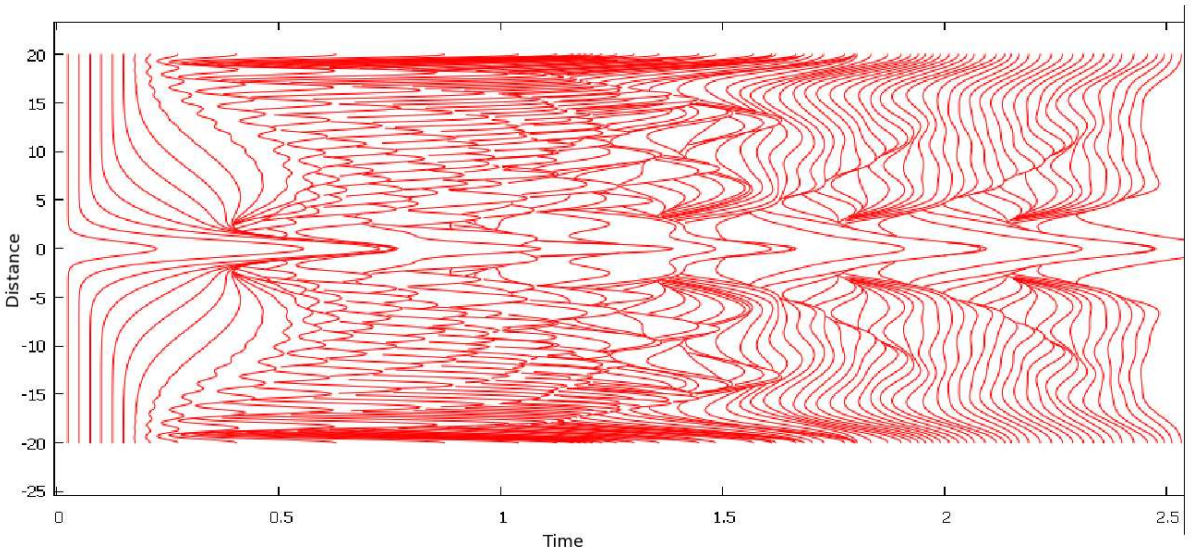

FIG. 17: 1st Harmonic excitation from a source at $\omega = 0.5$. Fronts form at early times at the fundamental similar to the uncoupled case.

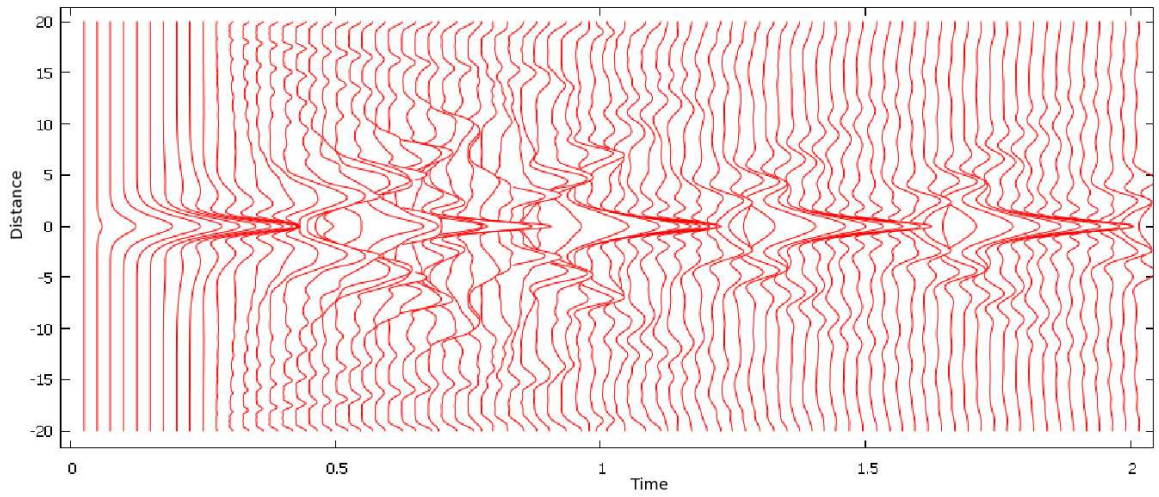

FIG. 18: 3rd Harmonic shows localization near the drive, but low amplitude solitons are generated that propagate toward the boundaries.

Here we have assumed an approximate varactor characteristic given by

$$C = C_0 + C_1 \tanh \beta V \tag{25}$$

where C_0, C_1 and β are parameters. However, the saturation characteristics of the capacitance at large voltages values do not impact the small signal system behavior appreciably, so we have replaced this characteristic by the Taylor expansion to second order

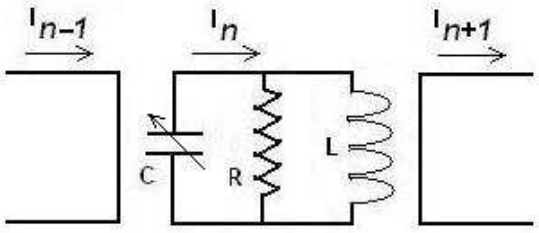

FIG. 19: Varactor circuit showing nonlinear capacitance varying with applied voltage.

$$\frac{1}{C} = \frac{1}{C_0} - \frac{\beta C_1}{C_0} V + \frac{\beta^2 C_1^2}{C_0^3} V^2 + \cdots \tag{26}$$

and this term introduces a nonlinear frequency shift into the system. It is clear from Eq. 24 that the only steady state solution is the trivial one at $A = 0$. As such, we find through numerical studies of Eq. 24 that there are no solitary waves of particular interest for this system. Indeed, the response is largely localized where the drive exists, and the travelling waves of the tunnel diode case do not occur. This result can be traced back to the fact we have only retained second-order spatial derivatives through the nearest-neighbor interactions, Eq. 13 and truncated the Taylor expansion, Eq. 26, to lowest order. In principle, higher-order derivatives can reintroduce travelling waves, which have been studied in the context of nonlinear transmission lines [7], and for metamaterial arrays in Refs. [13–15]. Because these concepts have already been treated in the literature, we will focus in this work on the frequency mixing aspects of such systems. The study of this behavior requires the inclusion of harmonic coupling driven by an external source, as given for the three-frequency case by

$$i\omega \dot{A}_1 + (\omega_0^2 - \omega^2) A_1 + i\omega\gamma A_1 = 2\omega_0^2 \frac{i\omega\beta C_1}{C_0} (A_2 A_1^* + A_0 A_2^*) \tag{27a}$$

$$2i\omega \dot{A}_2 + (\omega_0^2 - 4\omega^2) A_2 + 2i\omega\gamma A_2 = \omega_0^2 \frac{\beta C_1}{C_0} (2A_0 A_1^* + A_1^2) + 2i\omega\beta\gamma \frac{C_1}{C_0} A_1^2 \tag{27b}$$

$$\tag{27c}$$

To obtain this result, we have dropped higher order terms in β, which is assumed to be a small parameter, and we have assumed the array is driven at the third harmonic with amplitude A_0. Down-converted power from the third harmonic feeds both the second harmonic and fundamental terms. However, power is also upconverted from the fundamental to the second harmonic by the nonlinearity. It is noted that these expressions in the steady-state limit are similar to the Manley-Rowe relations [37], but include losses, and these results have been anticipated in this context by the work of Syms, et. al. [38] and Lapine et. al. [39]. The steady-state power in each harmonic may be computed by the algebraic solution of Eq. 27 with the time derivative terms set equal to zero.

We note also that the mixing of negative and positive frequency components as given by Eq. 27 can result in phase conjugation, a concept that has been described in the work of Katko, et. al. [40]. They point out that such a phenomenon can give rise to the practically useful time reversal of an incident wave.

It is worthwhile to consider the question whether varactor circuits are subject to chaotic behavior, owing to the presence of a nonlinear frequency shift. Considering only the fundamental behavior given by Eq. 24, we are led to the following pair of equations for the amplitude and phase of the envelope A

$$\dot{R} = -\gamma(R + R^3) + \varepsilon \cos(\Omega t + \theta) \tag{28a}$$

$$\dot{\theta} = \alpha + \Delta R^2 + \varepsilon \sin(\Omega t + \theta) \tag{28b}$$

where $\gamma = 1/(RC_0)$, $\alpha = (\omega_0^2 - \omega^2)/\omega$ and $\Delta = (\omega_0^2 + \omega^2)/\omega$. The key difference between Eq. 28 and Eq. 10 is the presence of the nonlinear amplitude dependence in the phase equation. This can lead to chaotic behavior in certain parameter regimes, as shown in Figs. 20. To elucidate this case, we have used a Runge-Kutta integration procedure in the time domain on the dynamical equations to examine the driven case. However, we use the complete description of the circuit given in Eq. 23 and 25 to describe the expected strong harmonic coupling.

In Fig. 21, we show that the circuit can exhibit chaotic behavior when the drive amplitude is increased beyond a certain threshold. We assert that this is true chaos in this case because of the absence of well-defined lines in the spectral response. Such behavior is derivable from Eqs. 28, but we find it more convenient to study the exact varactor characteristic curve numerically.

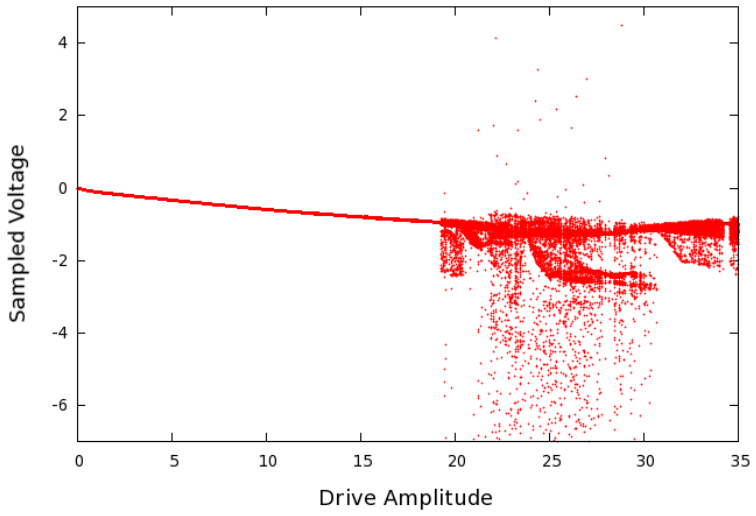

FIG. 20: Poincaré surface of section for the varactor case determined numerically. An abrupt transition into chaotic operation occurs at sufficiently high drive amplitudes, approximately $\epsilon = 18$.

VI. DISCUSSION

We have shown in the preceding sections that there is a wide diversity in nonlinear phenomena that can occur on an array of nonlinear oscillators. These phenomena can be categorized by either active or passive media. The former case is characterized by the presence of gain, or free energy, which gives rise to self-oscillations. The self oscillations can become synchronized by an external source, or may exhibit multiple frequencies, i.e. quasiperiodic behavior, if the external drive frequency is sufficiently detuned from the self-oscillation frequency. Moreover, for a given spatially or temporally localized illumination, the

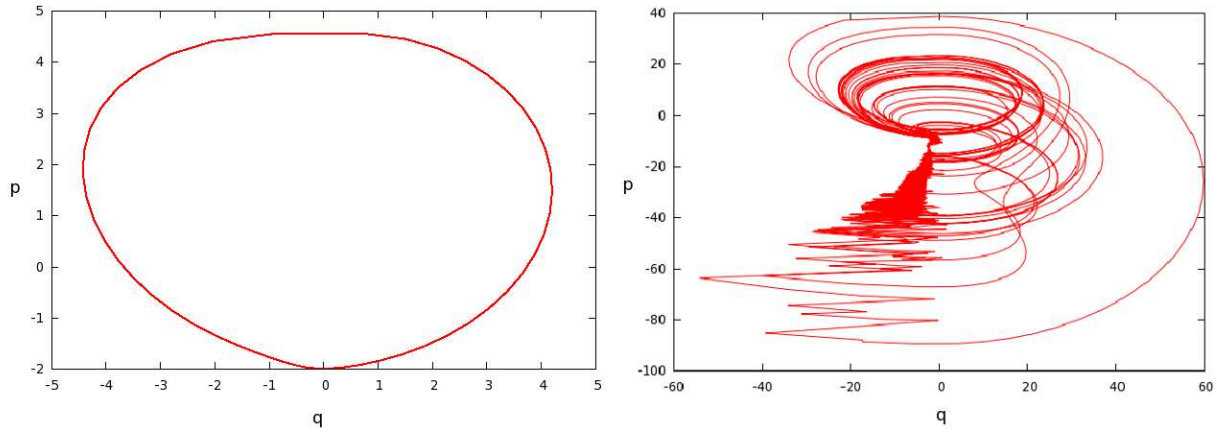

FIG. 21: Phase plane plots for (a) varactor case with low drive amplitude $\epsilon = 5$ and (b) above the Hopf bifurcation, $\epsilon = 25$, showing chaotic behavior.

medium can exhibit both fronts and solitons as it approaches a nonzero steady-state solution. Numerical studies suggest that there is a gain-dependent instability which may produce copious harmonic generation.

In the passive case, little of the exotic nonlinear wave phenomena persists that is evident in the active case. As we have noted, however, nonlinear waves can arise if higher-order corrections are retained in the cell dynamics. Moreover, for a medium driven by an external source, rich harmonic generation can occur, albeit localized to the spatial extent of the illumination. The behavior of an array of such nonlinear cells can be well characterized by the behavior of a single cell. For sufficiently nonlinear elements such as varactors driven in the large-signal limit these cells can exhibit clearly chaotic states.

It is worthwhile to make a few comments regarding the approach we have taken here. The well-known multiple time scale expansion given in Sec. III A is fundamentally an asymptotic method, valid when there exists a large difference between the fast and slow time scales. It can represent the behavior of the system once the initial transients have all decayed away. As such, it is difficult to predict the onset of true chaos where the phase, or in particular the phase gradient, may rapidly change on the fast time scale. Nonetheless, our method can be expected to delineate the parameter regimes where Hopf bifurcations occur that mark phase changes in the overall behavior of the nonlinear medium.

One particular restriction of this work is the assumption of identical, isotropic nonlinear cells. However, this is not a fundamental issue and may be modeled by introducing an ensemble average over a presumed distribution of cell frequencies. Such a situation leads to the notion of a coherence time, or coherence length, over which the synchronized states may lose phase lock. Indeed, operation outside the synchronized regime described previously leads to a rapid decoherence of the cells. In this limit, a useful approach is to assume a randomly-phased ensemble of oscillators, which may be modeled in a manner similar to that used in weak turbulence theory [41]. The object of this approach is to produce a spectral balance equation that describes the flow of power among all normal modes of the system and their harmonics. As in the case we have considered in this work, the analysis is based on weak coupling between cells and the existence of two very disparate time scales. We will leave this study to a future work.

We note that we have not extensively discussed applications of the phenomena that we have described here. In fact, we expect that the occurrence of synchronization will play an important role as it greatly enhances the

collective scattering behavior from such arrays. Moreover, the existence of macroscopic nonlinear structures can play a role in transferring information from one part of the array to another. Also of interest is the parametric control of harmonic content and chaotic states. Finally we wish to note that such arrays of nonlinear oscillators are ubiquitous throughout physics and engineering, and the ability to monitor behavior simultaneously at both the cell and array level in metamaterials may lead to deeper insight of similar phenomena that occur in other media.

Acknowledgments

The authors gratefully acknowledge support from Los Alamos National Laboratory Grant LDRD 20110027DR and helpful and stimulating discussions with Diego Dalvit, Yong Zeng, Larry Cox, Charles Bunting and Prof. Alejandro Aceves. LA-UR-12-24087.

---

[1] D. Schurig, J. J. Mock, B. J. Justice, S. A. Cummer, J. B. Pendry, A. F. Starr, and D. R. Smith, Science **314**, 977 (2006).
[2] A. Erentok and R. W. Ziolkowski, IEEE Trans. Antennas Propag. **56**, 691 (2008).
[3] J. F. O'Hara, R. Singh, I. Brener, E. Smirnova, J. Han, A. J. Taylor, and W. Zhang, Optics Express **16**, 1786 (2008).
[4] J. Pendry, Phys. Rev. Lett. **85**, 3966 (2000).
[5] H. T. Chen, J. F. O'Hara, A. K. Azad, A. J. Taylor, R. D. Averitt, D. B. Shrekenhamer, and W. J. Padilla, Nature Photonics **2**, 295 (2008).
[6] P. Milonni, M.-L. Shih, and J. Ackerhalt, *Chaos in laser-matter interactions, World Scientific Lecture Notes in Physics*, vol. 6 (World Scientific, 1987).
[7] M. Lin and W. Duan, Chaos, Solitons and Fractals **24**, 191 (2005).
[8] E. Fermi, J. Pasta, and S. Ulam, LASL Report **1940** (1955).
[9] G. P. Berman and F. M. Izrailev, Chaos **15**, 015104 (2005).
[10] J. C. Sprott, *Chaos and Time Series Analysis* (Oxford University Press, 2003).
[11] I. Aronson and L. Kramer, Rev. Mod. Phys. **74**, 99 (2002).
[12] A. Zharov, I. Shadrivov, and Y. Kivshar, Physical Review Letters **91**, 037401 (2003).
[13] N. Lazarides, M. Eleftheriou, and G. P. Tsironis, Physical Review Letters **97**, 157406 (2006).
[14] M. Eleftheriou, N. Lazarides, and G. P. Tsironis, Physical Review E **77**, 036608 (2008).
[15] P. Giri, K. Choudhary, A. S. Gupta, A. K. Bandyopadhyay, and A. R. McGurn, Physical Review B **84**, 155429 (2011).
[16] V. M. Agranovich, Y. R. Shen, R. H. Baughman, and A. A. Zakhidov, Phys. Rev. B,**69**, 165112 (2004).
[17] A. Chowdhury, and J. A. Tataronis, Phys. Rev. Lett., **100**, 153905 (2008).
[18] A. K. Popov, European Physics Journal D **58**, 263 (2010).
[19] M. Scalora, G. D'Aguanno, M. Bloemer, M. Centini, D. de Ceglia, N. Mattiucci, and Y. S. Kivshar, Opt. Express, **14**, 4746 (2006).
[20] A. Rose, D. Huang, and D. R. Smith, Phys. Rev. Lett., **107**, 063902 (2011).
[21] S. Longhi, Waves in Random and Complex Media, **15**, 119 (2005).
[22] G. D'Aguanno, M. Mattiucci, M. Scalora, and M. J. Bloemer, Phys. Rev. Lett., **93**, 213902 (2005).
[23] P. Chen, M. Farhat, and A. Alu, Phys. Rev. Lett., **106**, 105503 (2011).
[24] L. O. Chua, T. Matsumoto, and M. Komuro, IEEE Trans. on Circuits and Systems **32**, 798 (1985).
[25] J. O'Hara, M., Reiten, and P., Colestock, Proc. SPIE Conf. on Optics + Photonics, San Diego, CA (2011).
[26] A. Ruehli, IEEE Trans. on Microw. Theory Tech. **22**, 216 (1974).
[27] G. Antonini, D. Deschrijver, and T. Dhaene, IEEE Trans. on Electromagnetic Compatibility **49**, 35 (2007).
[28] G. Wollenberg and S. Kochetov, Intl. J. for Comp. and Math. in Electrical and Electronic Eng. **30**, 1283 (2011).
[29] Pikovsky, *Synchronization – A Universal Concept in Nonlinear Science* (Cambridge University Press, 2001).
[30] S. H. Strogatz, Physica D, **143**, 1 (2000).
[31] P. G. Drazin, *Nonlinear Systems* (Cambridge University Press, 1992).
[32] N. M. Krylof and N. N. Bogoliubov, *Introduction to Nonlinear Mechanics* (Princeton University Press, 1943).
[33] I. Shadrivov, A. Zharov, N. Zharova, and Y. Kivshar, Photonics and Nanostructures - Fundamentals and Applications **4**, 69 (2006).

[34] W. Saarloos and P. C. Hohenberg, Physica D **56**, 303 (1992).
[35] T. B. Benjamin, Proceedings of the Royal Society of London A: Mathematical and Physical Sciences **299**, 59 (1967).
[36] FlexPDE6, PDE Solutions Inc., URL `www.pdesolutions.com`.
[37] J. M. Manley and H. E. Rowe, Proceedings of the Institute of Radio Engineers **44**, 904 (????).
[38] R. R. A. Syms, L. Solymar, and I. R. Young, Metamaterials **2**, 122 (2008).
[39] M. Lapine and M. Gorkunov, Phys. Rev. E **70**, 066601 (2004).
[40] A. Katko, S. Gu, J. Barrett, B. Popa, G. Shvets, and S. Cummer, Phys. Rev. Lett. **105**, 123905 (2010).
[41] R. Z. Sagdeev and A. A. Galeev, *Nonlinear Plasma Theory* (W. A. Benjamin, New York/London, 1969).

Appendix A: Averaging the Dynamical Equations for a Cell

We wish to consider the asymptotic properties of a nonlinear resonator near the point where a phase transition may occur, namely when it may break into self-oscillations when the gain of the tunnel diode just compensates for the resistive losses of the system. This condition is tantamount to a phase transition and the system naturally breaks into a fast time scale over which the oscillator phase changes and a slow time scale over which the amplitude of the oscillations may vary. For convenience, we repeat here the equations for a single tunnel diode-loaded cell:

$$\dot{p} = -q - \gamma p + \alpha_3 p q^2 \tag{A1a}$$
$$\dot{q} = p \tag{A1b}$$

Without loss of generality, we have shifted the origin of q to symmetrize the potential and we have normalized the resonant frequency to unity. Formally, this system exhibits a phase change when γ changes sign, namely at the onset of self-oscillation. We wish to study this phenomena in the vicinity of the transition, that is when γ is presumed to be small, and we will show that $1/\gamma$ is associated with the slow time scale and by assumption we have $1/\gamma \gg 1/\omega_0 = 1$.

Two related asymptotic methods will be demonstrated. In the first method, the so called Poincaré-Linstedt approach [31], we will formally develop an expansion of the solution that is asymptotic in the parameter γ. The expansion leads to secularities, which however can be removed by appropriate choices of the free parameters introduced in the expansions. In the second approach [32], we introduce an envelope function which is assumed to be varying on a slow time scale compared to the phase variations. By averaging the equations over a cycle on the fast time scale, we may deduce a lower-order equation for the envelope. We will demonstrate both methods on the tunnel diode loaded cell in the following.

1. The Poincaré-Linstedt Method

We begin by transforming time in Eq. A1 by $\tau = \omega t$, where ω is a free parameter to be determined.

$$\omega p' = -q - \gamma p + \alpha_3 p q^2 \tag{A2a}$$
$$\omega q' = p \tag{A2b}$$

where the prime is the derivative with respect to τ. We now formally expand p, q and ω in a series of the form

$$p = \gamma^{1/2} p_{1/2} + \gamma p_1 + \gamma^{3/2} p_{3/2} + \cdots \tag{A3a}$$
$$q = \gamma^{1/2} q_{1/2} + \gamma q_1 + \gamma^{3/2} q_{3/2} + \cdots \tag{A3b}$$
$$A = \gamma^{1/2} A_{1/2} + \gamma A_1 + \gamma^{3/2} A_{3/2} + \cdots \tag{A3c}$$
$$\omega = \omega_0 + \gamma^{1/2} \omega_{1/2} + \gamma \omega_1 + \gamma^{3/2} \omega_{3/2} + \cdots \tag{A3d}$$

The expansion parameter is $\gamma^{1/2}$ which, as discussed above, is presumed to be small. Note that we have also expanded a quantity A, which is the arbitrary amplitude parameter that is associated with each order of the resulting solution. The validity of this expansion will be justified by the self-consistency of the resulting solutions. To proceed, we substitute A3 into A2 and gather terms separately for each order of $\gamma^{1/2}$. At the lowest order, we have

$$\omega_0 p'_{1/2} = -q_{1/2} \tag{A4a}$$
$$\omega_0 q'_{1/2} = p_{1/2} \tag{A4b}$$

We may arbitrarily shift the origin of this system to obtain the solution

$$\begin{aligned} p_{1/2} &= A_{1/2} \cos\frac{\tau}{\omega_0} \qquad & p'_{1/2} &= -\frac{A_{1/2}}{\omega_0} \sin\frac{\tau}{\omega_0} \\ q_{1/2} &= A_{1/2} \sin\frac{\tau}{\omega_0} \qquad & q'_{1/2} &= \frac{A_{1/2}}{\omega_0} \cos\frac{\tau}{\omega_0} \end{aligned} \tag{A5}$$

Now gathering terms of order γ, we have

$$\omega_0 p'_1 + \omega_{1/2} p'_{1/2} = -q_1 \tag{A6a}$$
$$\omega_0 q'_1 + \omega_{1/2} q'_{1/2} = p_1 \tag{A6b}$$

which leads to

$$\omega_0^2 p''_1 + p_1 = 2A_{1/2} \frac{\omega_{1/2}}{\omega_0} \cos\frac{\tau}{\omega_0} \tag{A7}$$

The long-time behavior of the solution is unbounded, which is known as a *secularity*, because the resonator described by the left hand side is being driven at resonance. However, since $\omega_{1/2}$ is a free parameter, we may remove the secularity by setting it to zero. This is the essence of the Poincaré-Linstedt method: secularities are removed order by order by setting the coefficients of resonant terms to zero. Gathering terms of order $\gamma^{3/2}$ we obtain

$$\omega_0 p'_{3/2} + \omega_1 p'_{1/2} = -q_{3/2} - p_{1/2} + \alpha_3 p_{1/2} q_{1/2}^2 \tag{A8a}$$
$$\omega_0 q'_{3/2} + \omega_1 q'_{1/2} = p_{3/2} \tag{A8b}$$

This leads to

$$\omega_0^2 p''_{3/2} + p_{3/2} = \frac{2\omega_1}{\omega_0} A_{1/2} \cos\frac{\tau}{\omega_0} + A_{1/2} \sin\frac{\tau}{\omega_0} \left[1 + \frac{\alpha_3 A_{1/2}^2}{2} \left(1 + 3\cos\frac{2\tau}{\omega_0} \right) \right] \tag{A9}$$

Removal of the secularities leads to the two conditions

$$\omega_1 = 0 \tag{A10a}$$

$$A_{1/2}^2 = \frac{4}{\alpha_3} \tag{A10b}$$

To this order, we have the following solution that is valid for all time

$$p = \gamma^{1/2} \frac{2}{\sqrt{\alpha_3}} \cos t \tag{A11a}$$

$$q = \gamma^{1/2} \frac{2}{\sqrt{\alpha_3}} \sin t \tag{A11b}$$

$$\omega_0 = 1 \tag{A11c}$$

which exhibits stable oscillations provided $\alpha_3 < 0$ and $\gamma < 0$. This is in essence the manifestation of the limit cycle behavior described in the text. In the next section we shall derive the same result using an averaging technique that is based on the same separation of time scales.

2. The Method of Averaging

A method due to Bogoliubov [32] that is valid for weak nonlinearities of the sort we are considering here begins with the ansatz

$$q = \frac{1}{2} \left(A \, \mathrm{e}^{i\omega t} + \text{c.c.} \right) \tag{A12}$$

where as before ω is a free parameter to be determined. Without loss of generality, we may define

$$\dot{q} = \frac{i\omega}{2} \left(A \, \mathrm{e}^{i\omega t} - \text{c.c.} \right) \tag{A13}$$

Upon substitution in Eq. A1, we average over a cycle of the fast time scale keeping A constant, from which we may deduce

$$i\omega \dot{A} - \omega^2 A = -A - i\omega\gamma A + \alpha_3 \frac{i\omega A}{4} |A|^2 \tag{A14}$$

For convenience we may take $\omega = 1$. We are interested in the steady-state solution which leads to the condition

$$-\gamma + \frac{\alpha_3}{4} A^2 = 0 \tag{A15}$$

which implies

$$A = \frac{2\gamma^{1/2}}{\sqrt{\alpha_3}} \tag{A16}$$

and this is the same result obtained by the Poincaré-Linstedt method as shown in Eq. A11.

The two methods described above differ in the frequency content of the higher-order contributions, *unless higher order harmonics are explicitly included in the ansatz of the form Eq. A12*, which we have outlined in the text. In that case the two methods give identical results.

In this paper we employ the Method of Averaging due to its relative ease of implementation. In all cases we shall be primarily interested in the long-time behavior of systems with very disparate time scales, as demonstrated by the above examples.

Appendix B: Derivation of the Nonlinear Coupling Terms

We wish to calculate the harmonic terms that contribute to a given harmonic in Eq. 20. We assume that the voltage is given by a series of the form $V_n = \phi + \phi^*$ where $\phi = \sum_{k=1}^{N} A_k \, \mathrm{e}^{ik\omega t}$. A typical expression from the nonlinear terms is given in the following

$$\phi^2 \phi^* = \sum_{j=1}^{N} A_j \, \mathrm{e}^{ij\omega t} \sum_{k=1}^{N} A_k \, \mathrm{e}^{ik\omega t} \sum_{l=1}^{N} A_l^* \, \mathrm{e}^{-il\omega t}$$

Selecting the n^{th} harmonic, we retain all terms such that $j + k - l = n$. Noting that the conjugate of each term also occurs in Eq. 20, we will also retain all terms such that $j + k - l = -n$, with an appropriate sign change. The results for the nonlinear terms of Eq. 20 are summarized below, for harmonics up to $N = 5$.

$\phi^2\phi^*$:

$n = 1$:

$$A_1^* A_1^2 + 2A_1 A_2 A_2^* + A_5^* A_3^2 + A_3^* A_2^2 + 2A_1 A_3 A_3^* + 2A_1 A_4 A_4^* + 2A_1 A_5 A_5^* + 2A_2 A_3 A_4^* + 2A_2 A_4 A_5^*$$

$n = 2$:

$$A_2^* A_2^2 + 2A_2 A_1 A_1^* + A_4^* A_3^2 + 2A_1 A_3 A_2^* + 2A_1 A_4 A_3^* + 2A_2 A_3 A_3^* + 2A_1 A_5 A_4^* + 2A_2 A_4 A_4^* + 2A_2 A_5 A_5^* + 2A_3 A_4 A_5^*$$

$n = 3$:

$$A_1^* A_2^2 + 2A_3 A_1 A_1^* + A_3^* A_3^2 + 2A_1 A_4 A_2^* + 2A_2 A_2 A_3^* + 2A_1 A_5 A_3^* 2A_2 A_4 A_3^* + 2A_2 A_5 A_4^* + 2A_3 A_4 A_4^* + 2A_3 A_5 A_5^* + A_5^* A_4^2$$

$n = 4$:

$$A_2^* A_3^2 + 2A_4 A_1 A_1^* + A_3^* A_3^2 + 2A_2 A_3 A_1^* + 2A_1 A_5 A_2^* + 2A_4 A_2 A_2^* + 2A_2 A_5 A_3^* + 2A_4 A_3 A_3^* + 2A_3 A_5 A_4^* + 2A_4 A_5 A_5^2 + A_4^* A_4^2$$

$n = 5$:

$$A_1^* A_3^2 + 2A_5 A_1 A_1^* + 2A_5 A_2 A_2^* + 2A_3 A_4 A_2^* + 2A_3 A_5 A_3^* + A_3^* A_4^2 + A_5^* A_5^2 + 2A_5 A_4 A_4^* + 2A_2 A_4 A_1^*$$

$n = -1$:

$$A_3^* A_1^2 + 2A_1 A_2 A_4^* + A_5^* A_2^2 + A_5^* A_5^2 + 2A_1 A_3 A_5^*$$

$n = -2$:

$$A_4^* A_1^2 + 2A_1 A_2 A_5^*$$

$n = -3$:

$$A_5^* A_1^2$$

ϕ^3 :

$n = 1, n = 2$: $\quad 0$

$n = 3$: $\quad A_1^3$

$n = 4$: $\quad 3A_1^2 A_2$

$n = 5$: $\quad 3A_2^2 A_1 + 3A_1^2 A_2$

$n < 0$: $\quad 0$